Communication

V-Groove Channel Waveguides and Mach–Zehnder Interferometer in Hyperbolic van der Waals $MoOCl_2$

Olga Matveeva *, Kirill Voronin, Maria Titova, Sergey Chikalkin, Andrey Vyshnevyy, Aleksey Arsenin, Valentyn Volkov

Posted Date: 6 May 2026

doi: 10.20944/preprints202605.0189.v1

Keywords: photonic integrated circuits; v-groove optical waveguides; channel polaritons; telecommunication; van der Waals material $MoOCl_2$; in-plane anisotropy in the visible range; hyperbolic plasmon polaritons; Mach–Zehnder interferometer

 doi:10.20944/preprints202605.0189.v1

Communication

V-Groove Channel Waveguides and Mach–Zehnder Interferometer in Hyperbolic van der Waals $MoOCl_2$

Olga Matveeva [1,*], Kirill Voronin [2], Maria Titova [3], Sergey Chikalkin [1,4], Andrey Vyshnevyy [1,5], Aleksey Arsenin [1,5] and Valentyn Volkov [5]

[1] Moscow Center for Advanced Studies, Kulakova str. 20, Moscow, 123592, Russia
[2] Donostia International Physics Center (DIPC), Donostia/San-Sebastián, 20018, Spain
[3] Laboratory of Programmable Functional Materials, Center for Neurophysics and Neuromorphic Technologies, Moscow, Russia
[4] Russian Quantum Center, Bolshoy Boulevard 30, bld. 1, 121205 Moscow, Russia
[5] Emerging Technologies Research Center, XPANCEO, Internet City, Emmay Tower, Dubai, United Arab Emirates
* Correspondence: matveevavolga99@gmail.com

Abstract

Miniaturization of photonic integrated circuits is a long-standing problem in optical engineering. Nowadays, the most promising material platform for integrated photonics are anisotropic van der Waals materials due to overcoming the light diffraction limit. Here, we numerically study v-groove channel waveguides formed in a 50-nm-thick slab of the in-plane hyperbolic in visible and near-infrared ranges van der Waals material $MoOCl_2$. At the telecom wavelength 1550 nm, a channel supports a guided mode with an effective index 1.0206 and a decay length of 13.7 μm. We also design a Mach–Zehnder-type interferometric layout with a maximum splitter angle of approximately 7° for demonstration of a possible practical application in a telecom range and in-plane angular channel modes propagation characteristics. We demonstrate that using $MoOCl_2$ instead of gold leads to a tenfold reduction in the linear dimensions of the photonic integrated circuit. Therefore, we envision that by combining the extraordinary material properties of $MoOCl_2$ with the v-shaped geometry of waveguides, one can make the integration density of photonic devices close to electronics.

Keywords: photonic integrated circuits; v-groove optical waveguides; channel polaritons; telecommunication; van der Waals material $MoOCl_2$; in-plane anisotropy in the visible range; hyperbolic plasmon polaritons; Mach–Zehnder interferometer

1. Introduction

One of the main challenges in modern optical engineering is the spatial scaling of photonic integrated circuit elements to sizes comparable to the characteristic base sizes of nanoelectronic components. A fundamental obstacle to the ultra-dense integration of all-optical devices is the diffraction limit, which sets the minimum size of the electromagnetic field localization region in traditional dielectric guide structures. The classical approach to overcoming the diffraction limit in visible and near-infrared ranges is based on the use of surface plasmon polaritons [1–5] excited at the interface between a dielectric and a noble metal. However, the use of isotropic plasmonic platforms still does not provide the required dimensions for an integrating circuit.

Highly anisotropic layered van der Waals crystals [6,7], which provide compatibility with planar technology, are currently being intensively studied as an alternative material base. The presence of hyperbolic in-plane dispersion of permittivity in such media allows the existence of electromagnetic eigenmodes [8] with large wave vectors—hyperbolic polaritons, characterized by deep subwavelength spatial confinement of the field. However, the practical application of most of the studied hyperbolic media, such as hBN [9] or α-MoO_3 [10,11], is spectrally limited to the mid-infrared

 doi:10.20944/preprints202605.0189.v1

range due to the phonon nature of their resonances. In this regard, $MoOCl_2$ [12–22], which is capable of supporting hyperbolic plasmonic polaritons in the technologically in-demand visible and near-infrared parts of the spectrum, has attracted particular attention.

Despite the intense study of the fundamental electrodynamic properties of $MoOCl_2$, the problem of efficient signal propagation in waveguiding structures [23] based on this material requires separate consideration. The influence of the transverse geometry of the waveguide on the dispersion and transport characteristics of guided modes in hyperbolic media remains insufficiently studied. The formation of traditional strip waveguides from layered crystals using nanolithography and reactive ion etching is accompanied by material degradation at the structure boundaries, which can lead to signal scattering.

In this context, the use of channel-type guiding structures—waveguides with a v-shaped cross-sectional profile—seems to be an electrodynamically and technologically viable solution. As in classical studies [24,25] examining channel plasmon modes in metals, the v-shaped geometry facilitates localization of the electromagnetic field within the channel, minimizing the influence of edge surface defects on the attenuation of plasmon-polaritons in $MoOCl_2$.

In this paper, we numerically study the guiding properties of v-shaped optical subwavelength channel waveguides based on the hyperbolic material $MoOCl_2$ and propose a computational model for a subwavelength Mach-Zehnder interferometer based on coupled channel waveguides.

2. Materials and Methods

In this work, we start with simulation of a v-shaped straight groove of width w and depth t, formed in a $MoOCl_2$ layer with a thickness of d = 50 nm and oriented along the [100] crystallographic axis. We consider the wavelength range of 360–1700 nm, where the dielectric permittivity tensor has a negative component along the [100] axis and positive components along the [010] and [001] axes, giving rise to a hyperbolic in-plane dispersion law.

Numerical calculations were prepared in COMSOL Multiphysics. $MoOCl_2$ was modeled as a biaxial dispersive medium with a diagonal dielectric tensor [15] in the crystallographic basis [100], [010], and [001]. The tensor orientation was changed throughout the simulations by in-plane rotation matrixes, while the propagation direction of the v-groove channel was kept fixed in order to find its eigenmodes.

3. Results

The groove plays a dual role: it reduces the characteristic transverse size of the mode and defines its direction of propagation within the plane of the structure. The field distribution in the cross-section (Figure 1a) demonstrates significant localization of the mode near the groove.

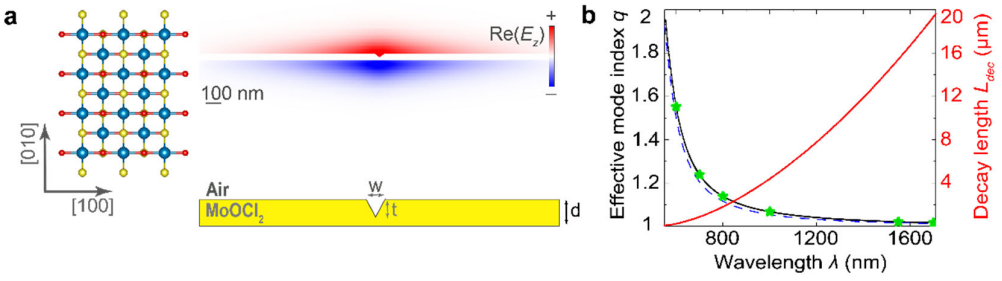

Figure 1. Channel mode in v-shaped waveguide based on $MoOCl_2$. (**a**) Atomic in-plane structure of $MoOCl_2$ (molybdenum atoms are shown in blue, oxygen in red, and chlorine in yellow), linear-scale field distribution of out-of-plane component Re(E_z) in the channel mode and schematic image of the structure. (**b**) Left-hand scale: dependency of the effective index of the fundamental mode q on the wavelength λ for a layer of thickness d = 50 nm (black solid line for full-wave simulations, blue dashed line for analytical calculations) and for channel

 doi:10.20944/preprints202605.0189.v1

mode (green stars, waveguide dimensions are d = 50 nm, w = 30 nm and t = 30 nm). Right-hand scale: dependency of the decay length L_{dec} in a layer of thickness d = 50 nm on the wavelength of incident light λ (solid red line).

The real part of the normalized wave number q and the decay length L_{dec} were considered as the main characteristics of the mode, parameters are given by:

$$q = \frac{k}{k_0},\ L_{dec} = \frac{\lambda}{2\pi Im(q)} \quad (1)$$

From the dependency of an effective mode index q on wavelength λ (Figure 1b), we see that this value is approximately identical for the fundamental mode of the layer [8] and for the channel mode within it, yielding values slightly greater than 1, indicating the subwavelength nature of the channel mode. Furthermore, calculation of the channel mode decay length for the telecommunication range of 1260–1625 nm shows that these waves propagate over distances of 8 – 15.5 μm, which are sufficient for engineering applications.

However, to develop functional elements of optical circuits, such as splitters, elliptical resonators and interference elements, it is necessary to form waveguides at arbitrary in-plane angles to the optical axes of the crystal. By the wavelength λ = 1550 nm, we studied the dependence of the channel mode effective index q on the angle α between the [100] axis of the crystal and the waveguide axis (Figure 2a). Having plotted an isofrequency curve for the same wavelength λ = 1550 nm (Figure 2b), we found that the maximum channel mode propagation angle α is 10°. It should be noted that channel modes also exhibit stronger light localization with increasing of angle α than the fundamental mode in the layer.

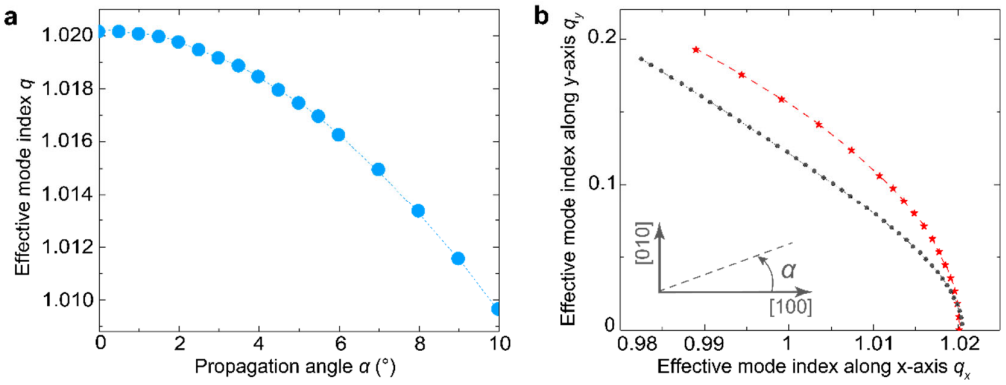

Figure 2. Angular dependency of the channel mode effective index. (**a**) Dependency of the effective index of the channel mode q on the angle α between [100] axis of $MoOCl_2$ and channel axis. (**b**) Isofrequency curve for the channel mode (red stars and interpolated dash line) and the fundamental slab mode (full-wave calculations, black points and interpolated dash line). Schematic image for channel in-plane direction (grey dashed line) defined by α in the inset. Wavelength λ = 1550 nm, parameters of the structure d = 50 nm, w = 30 nm and t = 30 nm for both (**a**) and (**b**).

To demonstrate its practical applicability, we simulated a model of a waveguide and a Mach-Zehnder interferometer based on it, performing a full-wave calculation at a wavelength of λ = 1550 nm. It was performed via numerical simulations to find the eigenmodes of the waveguide and calculate the normal component of the electric field Re(E_z) (Figure 3a, c) of waves propagating in the interferometer to visualize the interference pattern.

 doi:10.20944/preprints202605.0189.v1

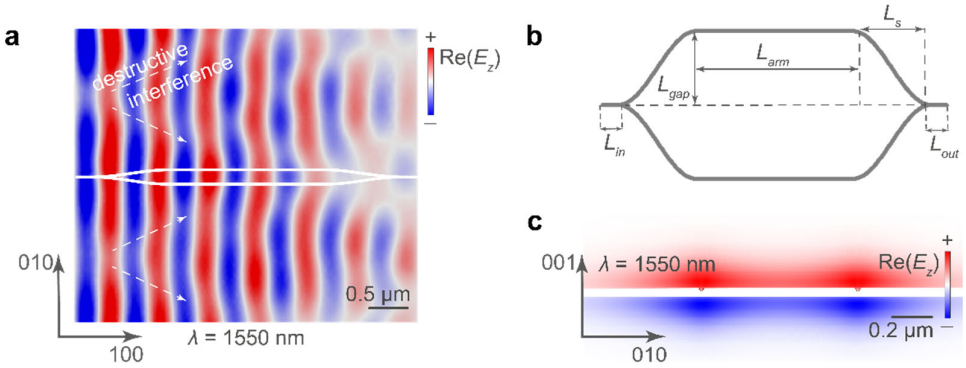

Figure 3. Mach-Zender interferometer based on $MoOCl_2$ slab. (**a**) Top-view and linear-scale field distribution of out-of-plane component Re(E_z). (**b**) Schematic image of interferometer (L_{in} = 500 nm, L_{gap} = 200 nm, L_{arm} = 2 μm, L_s = 2.5 μm, L_{out} = 500 nm). (**c**) Linear-scale field distribution of out-of-plane component Re(E_z) in the middle part of interferometer. Wavelength λ = 1550 nm, parameters of the waveguide w = 30 nm and t = 30 nm, layer thickness d = 50 nm for both (**a**) and (**c**). .

Efficient signal propogation along the interferometer requires adiabatic changes in the curvature of its arms, for which they are given an S-shape, defined by the function:

$$y(x) = \frac{L_{gap}}{2}(1 - \cos\frac{\pi x}{L_s}), \quad (2)$$

where x, y are the coordinates along the [100] and [010] axes. In addition, due to in-plane hyperbolicity, it is necessary that the maximum angle formed by the tangent to the function $y(x)$ and the x-axis does not exceed 10°. At this angle, the channel mode remains guided in the waveguide at a wavelength of λ = 1550 nm. Finding the derivative of this function and its maximum value, we see that the selected parameters (L_{in} = 500 nm, L_{gap} = 200 nm, L_{arm} = 2 μm, L_s = 2.5 μm, L_{out} = 500 nm) (Figure 3b) give the permissible value of the angle:

$$tg\alpha = \frac{dy}{dx} = \frac{\pi L_{gap}}{2L_s}\sin\frac{\pi x}{L_s},\ \alpha_{max} = arctg\left(\frac{\pi L_{gap}}{2L_s}\right) \approx 7° \quad (3)$$

The waveguide parameters w = 30 nm and t = 30 nm were chosen by varying them (Table 1A in the Appendix A section) in order to minimize the channel width and maximize the effective mode index q and its path length L_{dec}. To achieve the interference effect, L_{dec} must be guaranteed to exceed the interferometer arm length $L_{total} = L_{in} + L_s + L_{arm} + L_s + L_{out}$. In addition, the condition for the transfer coefficient $\frac{\Delta q}{q} \ll 1$ is satisfied everywhere on the bends.

4. Discussion

The comparative analysis (Table 1) demonstrates that the proposed $MoOCl_2$ platform instead of gold one enables to reduce (10-fold in in-plane dimensions, 25-fold in out-of-plane dimensions) the linear dimensions of the base elements while maintaining the efficiency of subwavelength signal propagation in the telecommunications range. To demonstrate the functional potential of the developed architecture, a computational model of a Mach-Zehnder interferometer based on coupled channel waveguides is proposed.

5. Conclusions

In conclusion, the obtained results demonstrate that the combination of the optical anisotropy of $MoOCl_2$ and the v-shaped geometry leads to significant approach of the photonic devices sizes to the standards of modern semiconductor electronics. More broadly, given recent advances in the fabrication [26–28] and nanostructure processing [29–31] of van der Waals materials, we anticipate that our findings will be used in next-generation integrated circuits, where van der Waals materials will complement traditional material platforms such as silicon [32–35].**Table 1.** Comparison of the

 doi:10.20944/preprints202605.0189.v1

liner geometrical parameters and propagation wavelength with other works (n = 1.02, λ = 1550 nm, v-shaped waveguide).

Criterion	Bozhevolnyi, S. I. et al. [24] Isotropic Model (Au)	This Work Anisotropic Model ($MoOCl_2$)
w and t, nm	277/1250	30/50
L_{dec}, μm	30	13.7

Author Contributions: A.A., V.V. and A.V. suggested and directed the project. O.M., K.V., M.T. and S.C. provided theoretical support. O.M. wrote the original manuscript with input of A.A. and A.V. All authors have read and agreed to the published version of the manuscript.

Funding: O.M. acknowledge the support from the Russian Science Foundation (grant №24-79-00308).

Data Availability Statement: The datasets generated during and/or analyzed during the current study are available from the corresponding author on reasonable request.

Conflicts of Interest: The authors declare no conflicts of interest.

Appendix A

It was found that for the geometric parameters listed in Table A1, the effective mode index q for λ = 1550 nm remains equal to 1.0206, indicating the weak sensitivity to the considered cross-sectional variations. For the interferometer simulation, we chose parameters w = 30 nm and t = 30 nm.

Table A1. The influence of the geometric parameters of the v-channel on the effective mode index q and the decay length L_{dec} for λ = 1550 nm during propagation along the [100] axis.

w and t, nm	Re(q)	Im(q)	L_{dec}, μm
60/30	1.0206	0.01807	13.650
60/45	1.0206	0.01809	13.635
120/45	1.0206	0.01818	13.569
30/30	1.0206	0.01806	13.662
120/30	1.0206	0.01811	13.621

In contrast to the telecom range, in the visible range we observe large losses and, as a consequence, short signal decay lengths. (Table A2).

Table A2. The influence of the geometric parameters of the v-channel on the effective mode index q and the decay length L_{dec} for λ = 600 nm during propagation along the [100] axis.

w and t, nm	Re(q)	L_{dec}, nm
60/30	1.3948	1109
60/45	1.4043	1086
120/45	1.4434	1022
120/30	1.4112	1071

References

1. Raether, H. Surface Plasmons. *Springer-Verlag* **1988**.
2. Novikov, I.V. and Maradudin, A.A. Channel polaritons. *Phys. Rev. B* **2002**, *66*, 035403.
3. Barnes, W.L.; Dereux, A. and Ebbesen, T.W. Surface plasmon subwavelength optics. *Nature* **2003**, *424*, 824.

 doi:10.20944/preprints202605.0189.v1

4. Pile, D.F.P. and Gramotnev, D.K. Channel plasmon–polariton in a triangular groove on a metal surface. *Opt. Lett.* **2004**, *29*, 1069.
5. Gramotnev, D.K.; Bozhevolnyi, S.I. Plasmonics beyond the diffraction limit. *Nat. Photonics* **2010**, *4*, 83–91.
6. Basov, D.N.; Fogler, M.M. and de Abajo, F.J.G. Polaritons in van der Waals materials. *Science* **2016**, *354*, aag1992.
7. Low, T. et al. Polaritons in layered two-dimensional materials. *Nat. Mat.* **2017**, *16*, 182-194.
8. Álvarez-Pérez, G.; Voronin, K.V.; Volkov, V.S.; Alonso-González, P. and Nikitin, A.Y. Analytical approximations for the dispersion of electromagnetic modes in slabs of biaxial crystals. *Phys. Rev. B* **2019**, *100*, 11.
9. Segura, A.; Artús, L.; Cuscó, R.; Taniguchi, T.; Cassabois, G. and Gil, B. Natural optical anisotropy of h-BN: highest giant birefringence in a bulk crystal through the mid-infrared to ultraviolet range. *Phys. Rev. Mat.* **2018**, *2*, 024001.
10. Ma, W. et al. In-plane anisotropic and ultra-low-loss polaritons in a natural van der Waals crystal. *Nature* **2018**, *562*, 557–562.
11. Zheng, Z. B. et al. A mid-infrared biaxial hyperbolic van der Waals crystal. *Sci. Adv*. **2019**, *5*, eaav8690.
12. Wang, Z. et al. Fermi liquid behavior and colossal magnetoresistance in layered $MoOCl_2$. *Phys. Rev. Mat.* **2020**, *4*, 041001(R).
13. Venturi, G.; Mancini, A.; Melchioni, N.; Chiodini, S. and Ambrosio, A. Visible-frequency hyperbolic plasmon polaritons in a natural van der Waals crystal. *Nat. Commun.* **2024**, *15*, 9727.
14. Ruta, F. L. et al. Good plasmons in a bad metal. *Science* **2025**, *387*, 786791.
15. Ermolaev, G. et al. Giant optical anisotropy and visible-frequency epsilon-near-zero in hyperbolic van der Waals $MoOCl_2$. *Nano Lett.* **2026**, *26*, 13.
16. Minnekhanov, A. Hyperbolic-enhanced Raman scattering in van der Waals $MoOCl_2$: from Fano resonances to picomolar detection. arXiv:2512.17647
17. Tong, H. $MoOCl_2$ as a hyperbolic planar platform for nanooptics at telecom frequencies. arXiv:2602.09186
18. Melchioni, N.; Mancini, A.; Nan L.; Efimova, A.; Venturi, G. and Ambrosio, A. Giant optical anisotropy in a natural van der Waals hyperbolic crystal for visible light low-loss polarization control. *ASC Nano* **2025**, *19*, 27.
19. Ermolaev, G. Deep-subwavelength and broadband quarter-wave retardation in ultrathin hyperbolic $MoOCl_2$. arXiv:2604.05236
20. Li, Y. et al. Broadband near-infrared hyperbolic polaritons in $MoOCl_2$. *Nat. Commun.* **2025**, *16*, 6172.
21. Melchioni, N.; Mancini, A.; Ambrosio, A. Anisotropic electron gas in a hyperbolic van der Waals material. arXiv:2602.01072.
22. Clemente-Marcuello, C. Launching of visible-range hyperbolic polaritons by gold nanoantennas in a natural van der Waals crystal. arXiv:2602.09180
23. Matveeva, O. G.; Voronin, K. V.; Grudinin, D. V.; Chikalkin, S. D.; Pak, N. V.; Titova, M. I.; Baranov, D. G.; Vyshnevyy, A. A.; Volkov, V. S.; Arsenin, A. V. Mode composition of waveguides based on a van der Waals crystal hyperbolic within the visible range. *Tech. Phys. Lett.* **2026**, *2*, 64.
24. Bozhevolnyi, S.I.; Volkov, V.S.; Devaux, E.; Ebbesen, T.W. Channel plasmon-polariton guiding by subwavelength metal grooves. *Phys. Rev. Lett*. **2005**, *95*, 046802.
25. Bozhevolnyi, S.I.; Volkov, V.S.; Devaux, E.; Laluet, J.-Y.; Ebbesen, T.W. Channel plasmon subwavelength waveguide components including interferometers and ring resonators. *Nature* **2006**, *440*, 508.
26. Liu, K.-K.; Zhang, W.; Lee, Y.-H.; Lin, Y.-C.; Chang, M.-T.; Su, C.-Y.; Chang, C.-S.; Li, H.; Shi, Y.; Zhang, H.; et al. Growth of large-area and highly crystalline MoS_2 thin layers on insulating substrates. *Nano Lett*. **2012**, *12*, 1538.
27. Najmaei, S.; Liu, Z.; Zhou, W.; Zou, X.; Shi, G.; Lei, S.; Yakobson, B.I.; Idrobo, J.C.; Ajayan, P.M.; Lou, J. Vapour phase growth and grain boundary structure of molybdenum disulphide atomic layers. *Nat. Mater*. **2013**, *12*, 754.
28. Dumcenco,D.; Ovchinnikov, D.; Marinov, K.; Lazi´c, P.; Gibertini, M.; Marzari, N.; Sanchez, O.L.; Kung, Y.-C.; Krasnozhon, D.; Chen, M.-W.; et al. Large-area epitaxial monolayer MoS_2. *ACS Nano* **2015**, *9*, 4611.

 doi:10.20944/preprints202605.0189.v1

29. Tselikov, G.I.; Ermolaev, G.A.; Popov, A.A.; Tikhonowski, G.V.; Panova, D.A.; Taradin, A.S.; Vyshnevyy, A.A.; Syuy, A.V.; Klimentov, S.M.; Novikov, S.M.; et al. Transition metal dichalcogenide nanospheres for high-refractive-index nanophotonics and biomedical theranostics. *Proc. Natl. Acad. Sci. USA* **2022**, *119*, e2208830119.
30. Munkhbat, B.; Yankovich, A.; Baranov, D.; Verre, R.; Olsson, E.; Shegai, T.O. Transition metal dichalcogenide metamaterials with atomic precision. *Nat. Commun.* **2020**, *11*, 4604.
31. Munkhbat, B.; Küçüköz, B.; Baranov, D.G.; Antosiewicz, T.J.; Shegai, T.O. Nanostructured transition metal dichalcogenide multilayers for advanced nanophotonics. *Laser Photonics Rev.* **2022**, 2200057.
32. Atabaki, A.H.; Moazeni, S.; Pavanello, F.; Gevorgyan, H.; Notaros, J.; Alloatti, L.; Wade, M.T.; Sun, C.; Kruger, S.A.; Meng, H.; et al. Integrating photonics with silicon nanoelectronics for the next generation of systems on a chip. *Nature* **2018**, *556*, 349.
33. Bogaerts, W.; Pérez, D.; Capmany, J.; Miller, D.A.B.; Poon, J.; Englund, D.; Morichetti, F.; Melloni, A. Prog rammable photonic circuits. *Nature* **2020**, *586*, 207.
34. Bogaerts, W.; Pérez, D.; Capmany, J.; Miller, D.A.B.; Poon, J.; Englund, D.; Morichetti, F.; Melloni, A. Programmable photonic circuits. *Nature* **2020**, *586*, 207.
35. Tanaka, Y. Recent progress in the development of large-capacity integrated silicon photonics transceivers. *IEICE Trans. Electron.* **2019**, *E102.C*, 357.